JACS
JOURNAL OF THE AMERICAN CHEMICAL SOCIETY
Article
pubs.acs.org/JACS

Controlled Electrodeposition of Bismuth Nanocatalysts for the Solution−Liquid−Solid Synthesis of CdSe Nanowires on Transparent Conductive Substrates

Natalia Reim, Alexander Littig, Dino Behn, and Alf Mews*

Institute of Physical Chemistry, University of Hamburg, 20146 Hamburg, Germany

ABSTRACT: Semiconductor nanowires (NWs) composed of cadmium selenide (CdSe) have been directly grown on transparent conductive substrates via the solution−liquid−solid (SLS) approach using electrodeposited bismuth nanoparticles (Bi NPs) as catalyst. Bi NPs were fabricated on indium tin oxide (ITO) surfaces from a bismuth trichloride solution using potentiostatic double-pulse techniques. The size and density of electrodeposited Bi NPs were controlled by the pulse parameters. Since the NW diameter is governed by the dimension of the Bi catalyst, the electrodeposition is a reliable method to synthesize nanowires directly on substrates with a desired size and density. We show that the density can be adjusted from individual NWs on several square micrometer to very dense NW networks. The diameter can be controlled between thick nanowires above 100 nm to very thin NW of 7 nm in diameter, which is well below the respective exciton dimension. Hence, especially the thinnest NWs exhibit diameter-dependent photoluminescence energies as a result of quantum confinement effects in the radial dimension.

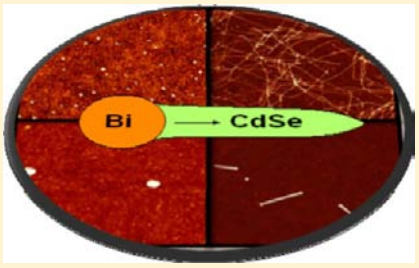

INTRODUCTION

During recent years, semiconductor nanowires have attained increasing attention due to their unique physical properties such as high surface-to-volume ratio and quantum effects, which led to extensive application as building blocks in nanoscale optoelectronics, transistors, and sensors.[1−5] For most of these examples, it is essential to control the diameter as well as the density of NWs on the surface. For example, a high density of nanowires is in great demand to construct large-scale devices such as photovoltaics and sensors.[6−10] In contrast, a low density of nanowires on substrates is mandatory for single nanowire devices, which detect individual events or single NW transistors.[11−13]

Semiconductor NWs are generally synthesized by employing metal nanoparticles as catalysts, while the precursors are either provided through the vapor phase[14] or the liquid phase.[15] Especially in the vapor−liquid−solid (VLS) approach, the catalyst particles are commonly deposited on substrates, and hence the NW growth is directly performed on the support. In contrast, in the solution−liquid−solid (SLS) approach, catalyst particles with a low melting point (mostly Bismuth particles) are dispersed in a solvent, and the NWs need to be separated from byproducts to be deposited on substrates.[16] However, there are few examples in which the SLS synthesis of nanowires can be performed directly on substrates. For example, it has been shown that the catalyst can be spin-coated on the surface[17] or thermally evaporated as a thin layer.[18−21] Subsequently, the substrate can be immersed in the reaction solution, where the NWs grow directly from the predeposited catalyst particles on the substrate. The major advantage of spin coating[16] is that the catalyst size can be adjusted by chemical methods beforehand and hence the diameter of the subsequently grown NWs. The nanowire growth with controlled diameter from substrates decorated with seed particles has been demonstrated for CVD and FLS methods, as well.[22−24] However, the catalyst particles are randomly distributed on the substrate similar to the growing nanowires thereof. In contrast, the evaporation of the thin metallic layers of catalyst material, which will transform into catalyst particles after thermal treatment, enables the growing nanowires on desired areas by photolithographic patterning of the metal thin film.[19] However, a metal evaporated film produces relatively large particles with a broad size distribution which results in nonuniform and relatively thick nanowires. Recently, CdSe NWs with narrow-diameter distributions were grown from the electrodeposited Bi thin films (2, 5, or 10 nm) with a new flow SLS technique.[25] Finally, small catalyst particles can also be directly formed on conductive substrates by electrochemical methods. Recently, we have shown that small Bi particles could be directly deposited on electrically contacted carbon nanotubes, which served as nanoscopic electrodes.[26] Subsequently, CdSe nanowires could be grown directly from these Bi particles using the SLS approach. From that study, we gained first indications that the size and density of electrochemically deposited Bi particles could possibly be controlled by the deposition method to finally adjust the diameter and concentration of subsequently grown nanowires on substrates.

Hence, in this study we employed the so-called double-pulse electrodeposition method to electrochemically prepare Bi nanocatalysts on ITO surfaces for subsequent preparation of CdSe nanowires. The double-pulse method is a well-established

Received: August 15, 2013
Published: November 18, 2013

   dx.doi.org/10.1021/ja408265s | J. Am. Chem. Soc. 2013, 135, 18520−18527

technique to control the density and size of the particle by applying a short nucleation pulse of high cathodic polarization followed by a longer growth pulse at low cathodic overvoltage.[27−33] We will show that this method can be utilized to prepare bismuth particles of varying density and size directly on ITO surfaces for the subsequent growth of CdSe nanowires.

RESULTS AND DISCUSSION

Double-Pulse Electrodeposition of Bi NPs. The density and diameter of nanowires directly grown on the substrates depend on density and size of bismuth nanocatalysts. Hence, the controlled electrodeposition is an efficient way to generate bismuth nanoparticles with diverse density and size on conductive surfaces and can be achieved by the potentiostatic double-pulse technique. In general, the method was first introduced by Scheludko and Todorova[34] and is based on the separation between the electrochemical nucleation and growth of particles on conductive surfaces. This is achieved by applying a sequence of two pulses, one of which is the nucleation pulse and the other one the growth pulse. Both pulses are characterized by their potentials ($E_{Nucl} > E_{Gr}$) and the corresponding pulse durations ($t_{Nucl} < t_{Gr}$), respectively. The first pulse (E_{Nucl}) lasts for a very short time interval (t_{Nucl}) of only several milliseconds and is used to initiate the formation of nuclei on the surface. Most important, its potential E_{Nucl} is more negative that the critical nucleation potential E_{Crit} at which particles could possibly nucleate at the surface. The second pulse (E_{Gr}) can last for several seconds (t_{Gr}) and is used to promote the growth of the nuclei formed during the previous nucleation pulse. The potential during this growth period needs to be more positive than E_{Crit}, such that no new nuclei are formed. On the other hand, the potential has to be more negative than the reversible potential at which the particles would redissolve upon oxidation.

In order to determine the respective potentials, we performed cyclic voltammetry measurements under similar experimental conditions, where the particle formation was achieved. Figure 1 below shows a cyclic voltammogram recorded to determine the electrochemical interaction of an ITO working electrode with a solution containing 1 mM $BiCl_3$, 50 mM KCl at pH 0.

The voltammogram shows two cyclic waves where the potential of the ITO was swept back and forth from +200 mV to −700 mV vs a standard calomel electrode (SCE) as a reference. The black solid line shows the first sweep, while the solid red line shows the consecutive second sweep. For each sweep, the negative current signals at negative potentials below −200 mV result from reductive deposition of the Bi onto the ITO surface, while the positive current at more positive potentials above −200 mV is due to oxidative dissolution of Bi ions into the solution. From the first sweep, it can be seen that the cathodic deposition of Bi on the ITO surface starts at a critical value of $E_{Crit} \approx -340$ mV. On the other hand, the second sweep indicates reductive deposition of Bi already at values less than −200 mV. This can be explained by assuming that the nucleation of Bi particles during the first sweep needs a larger (negative) overpotential than the growth of Bi on existing particles during the second sweep. This is surprising because the positive current signals at more positive potentials above −200 mV indicate that the Bi particles dissolve at least partially upon anodic oxidation. However, the shift of reductive deposition peaks toward less negative values indicates that only unstable crystals might dissolve and that the stable nuclei will grow further during the second cycle. In any case, especially the shape of the cathodic deposition peaks allows us to clearly distinguish between potential regimes for nucleation and growth. Here, we defined these regimes by using the crossovers values of the respective potential wave. The crossover of the black wave (first scan) at −340 mV is defined as the critical nucleation potential E_{crit} because nucleation can be achieved only at more negative potentials. The crossover of the red wave (second scan, −210 mV) is defined as the minimum growth potential because dissolution starts at more positive potentials. Hence, the potential for the nucleation pulse has to be adjusted at values more negative than −340 mV, while the growth potential should be adjusted between −210 and −340 mV.

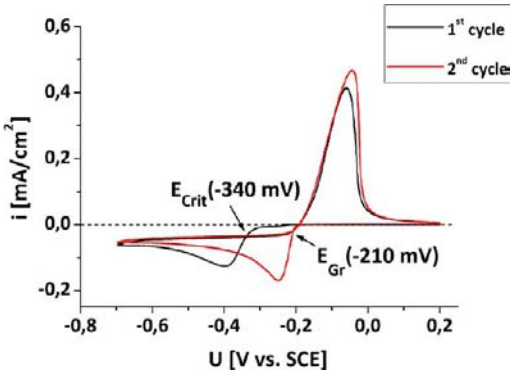

Figure 1. Cyclic voltammograms of ITO-covered glass in 1 mM $BiCl_3$ solution at scan rates of 50 mV s^{-1} (+200 to −700 mV). E_{Crit} denotes critical voltage and E_{Gr} growth voltage.

In the following, we will show results of Bi particle deposition on ITO substrates, where we systematically varied the nucleation voltage E_{Nucl} in the range of −400 to −600 mV at a fixed nucleation pulse length of t_{Nucl} = 20 ms. For each nucleation voltage, we also varied the growth time t_{Gr} between 0.25−1 s, while the growth voltage was kept constant at a value of −210 mV. The latter one was chosen on the basis of several preliminary experiments (not shown). Essentially, we found that small amounts of Bi ions can also be reduced on clean ITO surfaces at any potential below −200 mV, where the reduction rate is strongly dependent on the reducing potential. Hence, we picked a value of E_{Gr} = −210 mV close to the equilibrium potential, where the nucleation is strongly reduced and the Bi ions almost exclusively grow on exiting particles upon reduction.

AFM images of the samples with bismuth nanoparticles on the ITO substrates obtained by the described double-pulse electrodeposition are presented in the Figure 2, while respective height histograms from the same samples are shown in Figure 3. Two main trends protrude from the interdependence between applied voltage and growth time. An increase in the (negative) nucleation voltage leads to an increase in the particle density and a decrease in the particle size. For example, at a growth time of t_{Gr} = 0.5 s (middle row in Figures 2 and 3), there are only a few particles observed on an area of 25 μm^2 at a nucleation voltage of E_{Nucl} = −400 mV. This value increases to about 230 particles/25 μm^2 if the nucleation voltage increases to E_{Nucl} = −600 mV. At the same time, the mean diameter decreases from about 95 to 20 nm, as judged from the respective AFM height. The increase of particle density on the surface can be explained by assuming an activation of more sites at higher nucleation overpotentials. Since adjacent particles

dx.doi.org/10.1021/ja408265s | J. Am. Chem. Soc. 2013, 135, 18520−18527

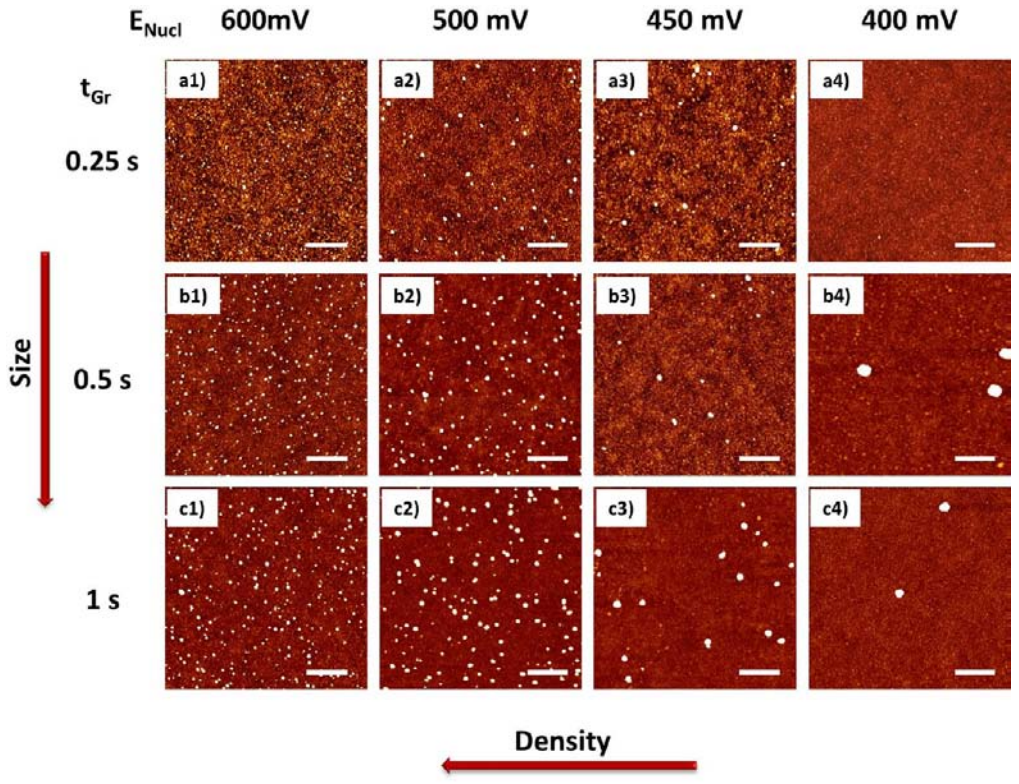

Figure 2. AFM images of Bi NPs on ITO substrates deposited in dependence of E_{Nucl} and t_{Gr}; t_{Nucl} = 20 ms and E_{Gr} = −210 mV were kept constant; (a1−a4) E_{Nucl} = −600, −500, −450, −400 mV, t_{Gr} = 0.25 s; (b1−b4) E_{Nucl} = −600, −500, −450, −400 mV, t_{Gr} = 0.5 s; (c1−c4) E_{Nucl} = −600, −500, −450, −400 mV, t_{Gr} = 1 s. All scale bars reflect 1 μm.

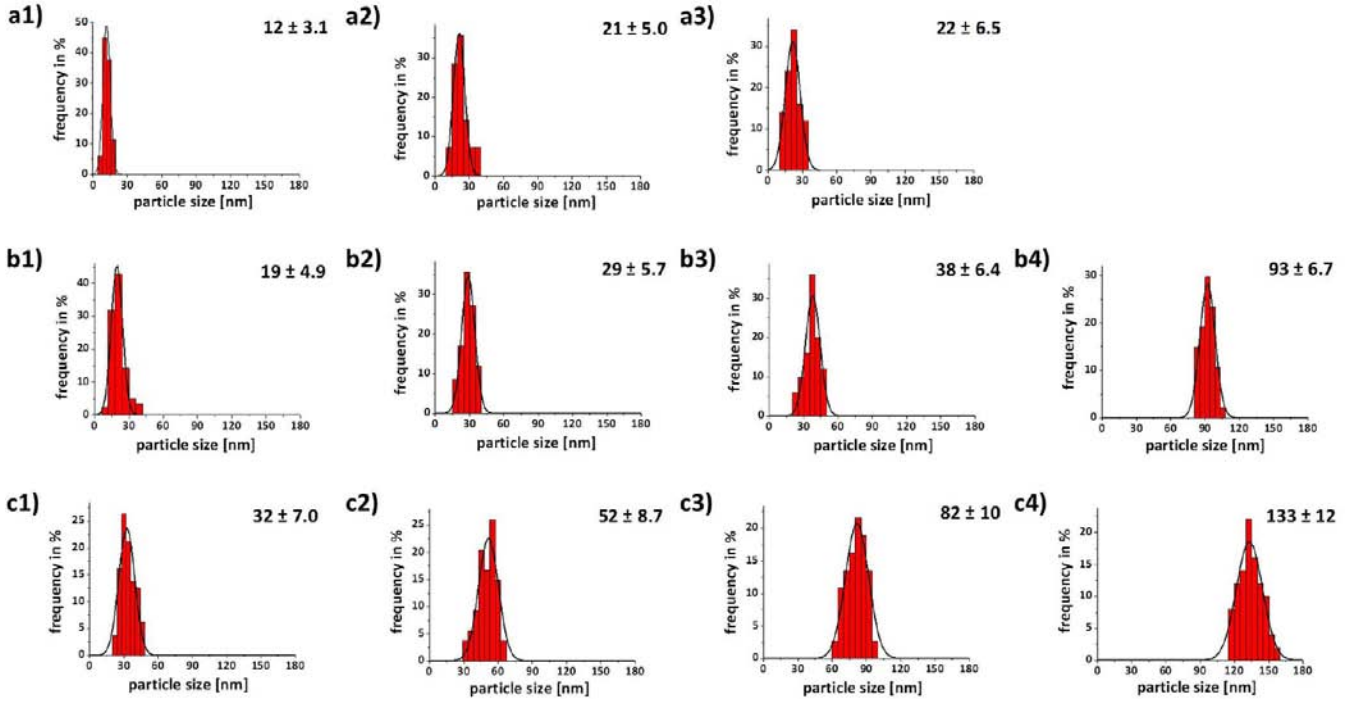

Figure 3. Particle size histograms of deposited BiNPs for samples with corresponding AFM images in Figure 2. (a1−a3) E_{Nucl} = −600, −500, −450 mV, t_{Gr} = 0.25 s; (b1−b4) E_{Nucl} = −600, −500, −450, −400 mV, t_{Gr} = 0.5 s; (c1−c4) E_{Nucl} = −600, −500, −450, −400 mV, t_{Gr} = 1 s.

compete for bismuth ions during the growth period, this results in the decrease of the particle size at larger densities.

The homogeneity of the particle density and size of electrodeposited particles by using the pulsed techniques has also been investigated by several other authors. For example, Terryn et al. suggested that the early nanoparticle growth can also be explained by a movement of nanoclusters and their aggregation on the surface.[35] They assumed that during the

dx.doi.org/10.1021/ja408265s | J. Am. Chem. Soc. 2013, 135, 18520−18527

nucleation pulse, the diffusion zones of the small clusters overlap provoking the surface movement of the clusters. Hence, the small clusters can aggregate with each other, forming a new large particle or grow through the direct attachment of ions. As a consequence, small nuclei where found to be surrounded by large particles in a satellite-like architecture resulting in heterogeneous particle size and density. Hence, in our case, the nucleation time was chosen to be only 20 ms to ensure that the satellite-like growth and formation of new nuclei can be prevented.

The final particle dimension is given by the growth time at −210 mV, following the respective nucleation pulses at different potentials and also by the density of the particles. For example, if the initial density is relatively low at nucleation potentials of −400 mV, the Bi particles grow to sizes larger than 100 nm. At high densities (e.g., at nucleation potentials of −600 mV), the final particle height is only in the range of 30 nm. This effect was investigated in detail by Penner et al.,[36,37] who developed a theory based on diffusion coupling between neighboring metal particles on the electrode surface. In essence, they showed that particles within densely nucleated areas grow more slowly than in regions with fewer particles. This is due to stronger depletion of ions, if the individual diffusion zones around individual particles start to overlap. If a small particle lies in the diffusion zone of a larger particle, the undersaturation can even favor the dissolution of the particle. Hence, during the growth pulse, the interparticle diffusion can also facilitate broadening of the size distribution.

CdSe NWs Synthesis Catalyzed by Electrodeposited Bi NPs. In the following, we will show that the electrodeposited bismuth nanoparticles on the ITO substrate can serve as a catalyst for nanowire growth by the SLS method. For this purpose, the reaction temperature needs to be carefully adjusted. If the reaction temperature is too low, the Bi particles will stay solid and have no catalytic activity for the SLS growth. If the temperature is too high, the particles will detach from the surface. In general, the requirements on the Bi particles to be catalytically active and remain attached to the surface are given close to the melting point. However, in our previous papers, we have shown that both requirements are fulfilled at different temperatures depending on the size of the Bi particles.[16,26] Hence, before use of the substrates with electrodeposited Bi particles for the catalyzed NW growth, the optimized reaction temperatures were determined.

For this purpose, the ITO substrates with diverse deposited Bi NPs were immersed into hot TOPO solutions at temperatures of 220, 250, and 270 °C, for 1 min each, and subsequently screened by AFM. We found that the particles having a size below 20 nm detach from the substrate already at 220 °C, while NPs between 20 and 30 nm detach between 220 and 250 °C and NPs bigger than 30 nm remain attached up to 270 °C (Table 1).

On this basis, the reaction temperature for the substrates with very small Bi particles (a1) was chosen to be 220 °C, while a temperature of 250 °C was used for the substrates a2, a3, b1, and b2. The growth from the remaining substrates with Bi particles larger than 30 nm was performed at a reaction temperature of 270 °C, close to the melting point of macroscopic bismuth of 271 °C.

An important synthesis step to grow NWs on a substrate is the sequence of the precursor injection. Best results in terms of yield and homogeneity were obtained if the Cd precursor was dissolved first followed by immersion of the Bi−ITO substrates

Table 1. Melting Behavior of Electrodeposited Bi NPs at Different Temperatures. Negative Sign Means That No Particles Were Observed on the ITO Substrate, While Positive Signs Indicate That the Particles Were Still Attached on the Substrate

	220 °C	250 °C	270 °C
$x < 20$ nm	−	−	−
20 nm $< x >$30 nm	+	−	−
$x > 30$ nm	+	+	−

and immediate injection of the Se precursor solution, as described in the experimental section below. In this way, a high local concentration of both precursors can be prevented in order to suppress the formation of isolated CdSe NPs.

AFM images (10 μm × 10 μm) of the resulting ITO substrates with the grown CdSe NWs are presented in Figure 4. The presence of Bi particles at the ends of the wires clearly confirms the NW growth by the SLS mechanism. However, it is also obvious that the number density of nanowires is smaller than the number of the initially deposited catalyst particles. This might partially be due to detachment of some Bi NPs from the surface at the necessary growth temperature to form CdSe-NW. On the other hand, it can also be seen in several AFM images with low NW concentrations (e.g., in a3, b3, and c3) that not all deposited Bi particles are catalytically active. Possible reasons might involve the formation of a passivating oxide layer on the Bi particles during the substrate cleaning step between the electrodeposition process and the subsequent NW growth procedure.

However, the density of the nanowires is mainly determined by the density of the initially deposited Bi NPs. This can be seen from the comparison of the AFM images of the CdSe NWs in Figure 4 with the respective AFM-images of the Bi particles in Figure 2, since the CdSe NWs were grown on the identical substrates. For example, a large density of Bi particles at high negative nucleation voltages (e.g., −600 mV) results in dense CdSe nanowire networks. On the other hand, low nucleation voltages of −400 or −450 mV result in low densities of Bi particles from which individual distinguishable CdSe wires can be grown.

From the corresponding AFM histograms in Figures 3 and 5 it can be seen that not only the density but also the diameter of CdSe NWs can be controlled through the electrochemical adjustment of the Bi NP size. Obviously, all resulting CdSe NWs are prepared with a relatively narrow diameter distribution of 10−20%, while the main diameter is controlled in a range from about 100 nm down to 7 nm, especially the thin NWs (a1−a3) extended over a length of several micrometers. A direct comparison of the AFM histograms of the NWs in Figure 5 with the corresponding Bi particles in Figure 3 reveals that the thin NWs are about 80% smaller in diameter than the respective Bi particles. As a result, CdSe NWs with a diameter of less than 7 nm could be observed, which is well below the bulk exciton diameter of CdSe (11 nm). Hence, the electrodeposition method allows preparing Bi particles which can produce true quantum wires, where the optical properties are clearly governed by quantization effects (see below).

For the thicker NWs between 15 and 30 nm, which are grown at 250 °C, and those with a diameter above 30 nm, which are grown at 270 °C, the diameter of the NWs is still about 20−30% smaller than the size of the corresponding Bi particles. Also, it can be seen that sometimes several thin wires

dx.doi.org/10.1021/ja408265s | J. Am. Chem. Soc. 2013, 135, 18520−18527

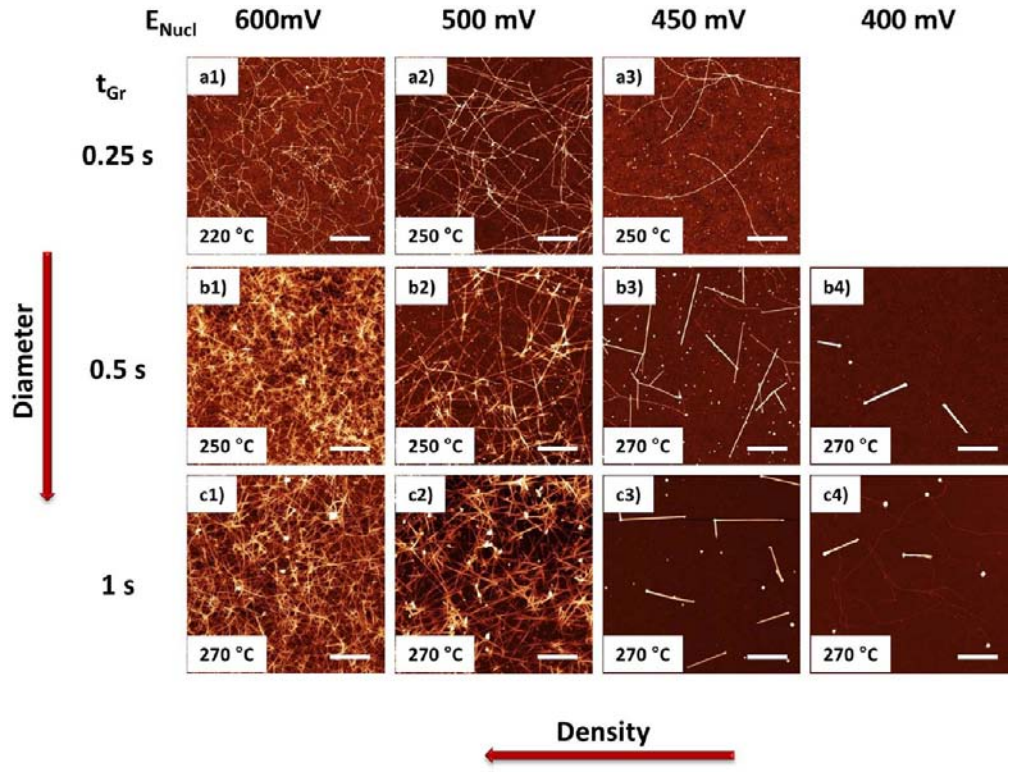

Figure 4. AFM images of CdSe NWs on ITO substrates grown from corresponding electrodeposited BiNPs in Figure 2; electrodeposition parameters: (a1−a3) E_{Nucl} = −600, −500, −450 mV, t_{Gr} = 0.25 s; (b1−b4) E_{Nucl} = −600, −500, −450, −400 mV, t_{Gr} = 0.5 s; (c1−c4) E_{Nucl} = −600, −500, −450, −400 mV, t_{Gr} = 1 s. All scale bars reflect 2 μm.

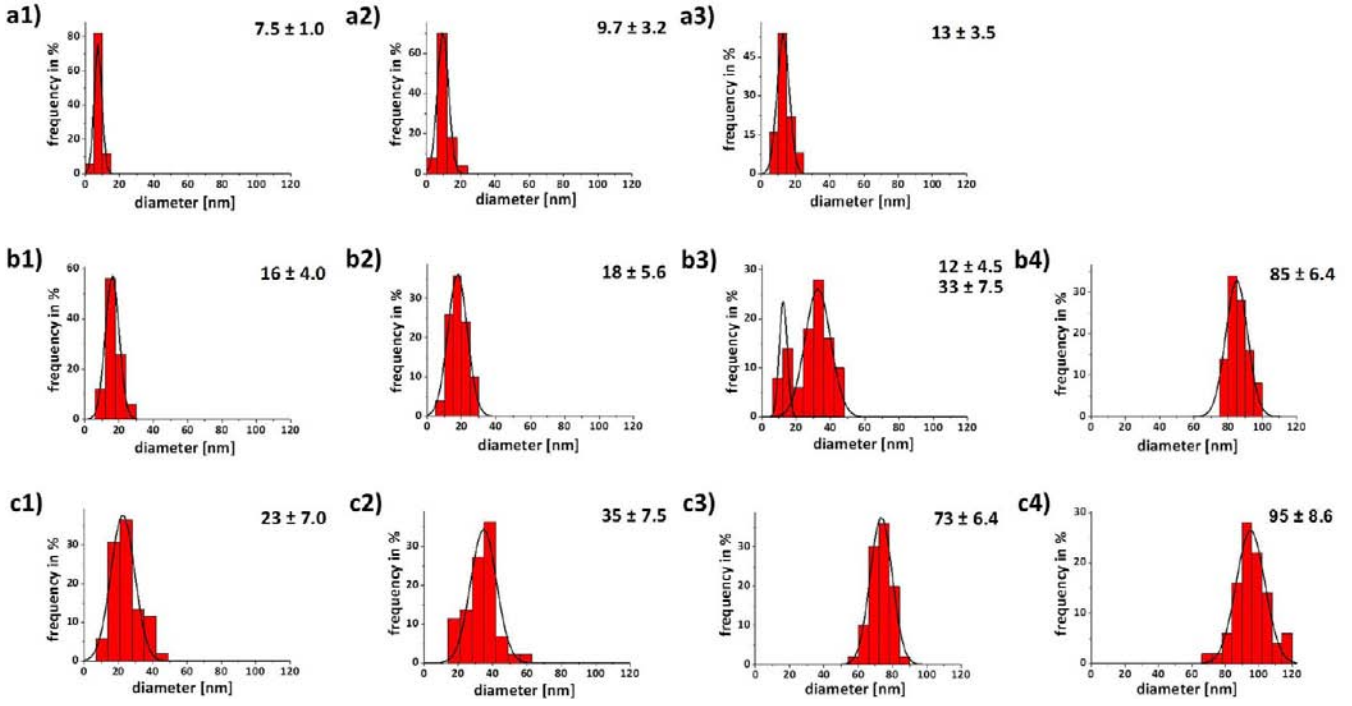

Figure 5. Diameter histograms of grown CdSe NWs for samples with corresponding AFM images in Figure 4. Electrodeposition parameters of BiNPs as catalyst: (a1−a3) E_{Nucl} = −600, −500, −450 mV, t_{Gr} = 0.25 s; (b1−b4) E_{Nucl} = −600, −500, −450, −400 mV, t_{Gr} = 0.5 s; (c1−c4) E_{Nucl} = −600, −500, −450, −400 mV, t_{Gr} = 1 s.

with a diameter about 10 nm were observed growing from one large Bi NP (e.g., b3 in Figures 4 and 5). A possible reason might be that corresponding catalyst particles were not completely molten or only partially catalytically active, mediated by a partially passivating oxide layer. However, as a general trend it can be observed that the thick NWs are considerably shorter than the thinner ones. This could simply be due to the fact that that the volume of those thick NWs is

dx.doi.org/10.1021/ja408265s | J. Am. Chem. Soc. 2013, 135, 18520−18527

much larger at a given length, which leads to a shorter wire at a given precursor feed. Another reason could be the competing reaction of CdSe nanocrystal formation in solution, which is much faster at high temperatures.

Besides the morphology (i.e., the diameter and length of the NW) we also investigated their spectroscopic properties by using fluorescence and Raman spectroscopy. Here, we used a confocal microscope and investigated only the samples, which were prepared by using a high nucleation voltage of −600 mV during the electrodeposition of Bi NPs, in order to determine the average spectroscopic properties. This high nucleation voltage of −600 mV ensured a high density of Bi particles and hence also a high density of the subsequently grown CdSe NWs.

In Raman spectroscopy, all samples showed two characteristic peaks at 206 and 411 cm^{-1}, as can be seen from the spectrum in Figure 6. The strongest mode at 206 cm^{-1} is

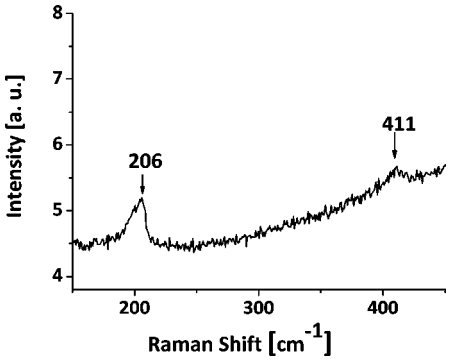

Figure 6. Typical Raman spectrum of CdSe NWs samples.

assigned to the first-order longitudinal optical phonon (LO), and 411 cm^{-1} is assigned to the second-order overtone 2 LO.[38] While this provides additional evidence for the presence of CdSe NWs on the surface, it also shows that the Raman spectra change only marginally with the diameter of the NWs.

In contrast, the photoluminescence spectra of the different substrates with NWs of different thickness are considerably different because the respective NWs exhibit a diameter-dependent quantum confinement effect in the radial wire dimension. Hence, the PL peaks from thin NWs are blue-shifted with respect to the wavelength of 716 nm, which would correspond to the photon energy expected for recombination of the electron−hole pair across the band gap in macroscopic CdSe (Figure 7). For example, the blue-shifted PL peak at 656 nm results from the nanowires with an average diameter of 7.5 nm, as shown in Figures 4a1 and 5a1, respectively. The corresponding Bi NPs were deposited using a growth time of only 250 ms and had an average height of 12 nm, as shown in Figures 2a1 3a1, respectively. With an increase in growth time, the Bi NPs became larger and consequently the nanowires are thicker. The subsequently synthesized NWs with a diameter of 12 nm were obtained from Bi NPs grown for 350 ms at −600 mV (AFM image not shown). The corresponding PL peak is at 709 nm. All wires with more than 12 nm in diameter show a PL wavelength close to the bulk PL peak at 716 nm. A representative sample for that case contains nanowires with a diameter of 23 nm, as shown in Figures 4c1 and 5c1, respectively.

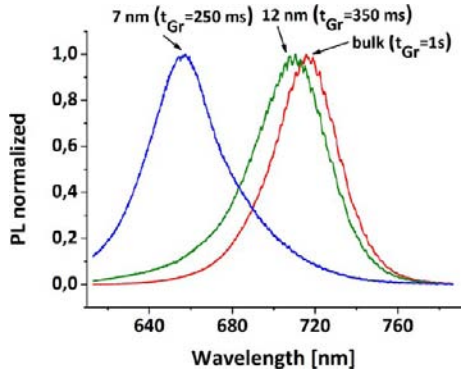

Figure 7. Normalized room temperature PL spectra for CdSe NWs with diameters of 7, 12, and 23 nm grown from electrodeposited Bi catalysts. Corresponding PL peaks (energies) are 656 nm (1.89 eV), 709 nm (1.75 eV), and 716 nm (1.73 eV), respectively.

CONCLUSION

In summary, we have demonstrated that nanowires can be directly synthesized on an ITO surface from electrodeposited bismuth catalyst particles. By using the double-pulse electrodeposition technique, we can control the size and the density of bismuth particles and hence the diameter and density of the subsequently grown NWs. In principle, this method could be applicable to all different kinds of nanowires materials which can be grown from Bi catalyst particles. Another advantage of this method is the possibility to grow nanowires with different density and size exclusively on conductive surfaces (e.g., patterned electrodes). Since the NWs are therefore directly electrically accessible, the method has an enormous potential to build thin film electrical or electro-optical devices such as sensors, photo detectors, or solar cells.

METHODS

Materials. Cadmium oxide (CdO, 99.99%), selenium powder (Se, 99%), and octanoic acid (OCA, 99%) were purchased from Aldrich. Tri-*n*-octyl phosphine oxide (TOPO, 99%) and trioctyl phosphine (TOP, 99%) were received from Merck and ABCR, respectively. Bismuth trichloride ($BiCl_3$, 99.99%) was obtained from Acros.

Electrodeposition of Bi NPs on ITO Substrates. Bi NPs were fabricated electrochemically on the transparent conductive substrates which were composed of thin layer of ITO (50 nm) on glass substrates with a thickness of 0.145 mm (Präzisions Glas and Optik GmbH, sheet resistance R_s = 20 ± 5 Ohm/sq). Prior to metal deposition, the ITO substrates were degreased by subsequent sonication for 15 min in acetone, isopropanol, and deionized water. For reducing the resistivity and sensibility to acids, the substrates were then annealed in a quartz furnace tube at 250 °C for 30 min under argon atmosphere. An electrical contact was established via copper strip which was glued with a conductive adhesive on ITO. Cyclic voltammetry studies and electrodeposition of Bi NPs on ITO substrates were performed in a three-electrode arrangement using a HEKA model PG310 potentiostat/galvanostat. Here, the ITO substrate served as the working electrode, and a standard calomel electrode (SCE) and Pt foil functioned as the reference and counter electrode, respectively. The aqueous bismuth electrolyte used contained 1 mM $BiCl_3$, 1 M HCl, 50 mM KCl and was purged with Ar for 20 min in order to remove dissolved oxygen. The Bi NPs were electrodeposited via the

dx.doi.org/10.1021/ja408265s | J. Am. Chem. Soc. 2013, 135, 18520−18527

potentiostatic double-pulse technique. Typical values for the pulse parameters were as follows: E_{Nucl} = −600 to −400 mV vs SCE; t_{Nucl} = 20 ms; E_{Gr} = −210 mV vs SCE; t_{Gr} = 250 ms−2 s. Afterward, the sample was washed with DI water.

Growth of CdSe Nanowires Using Deposited Bi NPs as Catalyst. CdSe NWs were synthesized by the Bi-seeded SLS growth method according to the procedures we previously reported.[16,26,39−41] First, cadmium and selenium precursor stock solutions were freshly prepared. A 2 M TOPSe stock solution was obtained by dissolving Se into trioctyl phosphine (TOP) under air-free conditions. For the cadmium precursor, 0.0025 M CdO and 1.5 mL octanioc acid (OCA) were loaded into a 50 mL three-neck flask, degassed under vacuum, and backfilled with nitrogen (three times). TOP (3.5 mL) was added, and the solution was then heated to 250 °C. The solution turned clear and colorless upon formation of the Cd−OCA complex. The cadmium precursor solution was cooled to room temperature and stored in the glovebox for further use. After the preparation of precursor stock solutions, 4 g of trioctyl phosphine oxide (TOPO) was loaded in a four-neck flask and evacuated over the course of 1 h at 100 °C. It was then backfilled with nitrogen and heated to the desired growth temperature ranging from 220 to 270 °C, relating to the size of Bi NPs. At the reaction temperature, 200 μL of 0.5 M cadmium precursor $Cd(OCA)_2$ stock solution were first injected into the TOPO solution, followed by the immersion of the Bi-electrodeposited ITO substrate with self-made Teflon holder and immediate injection of 50 μL of 2 M TOPSe, keeping the ratio of Cd/Se as 1:1. After 2 min, the substrate was taken off the solution and rinsed with toluene to remove TOPO and byproducts such as deposited CdSe nanoparticles.

Characterization. The ITO substrates with the electrodeposited Bi NPs as well as CdSe NWs on the surface were characterized by a Nanowizard II atomic force microscope from JPK Instruments operated in tapping mode. Photoluminescence (PL) and Raman spectra were recorded at room temperature using a home-built confocal laser scanning microscope. The sample was placed on top of an inverted microscope (Zeiss Axiovert 200) and illuminated from its back side with an Ar^+-laser operated at 488 nm.[42]

AUTHOR INFORMATION

Corresponding Author

*E-mail: mews@chemie.uni-hamburg.de.

Notes

The authors declare no competing financial interest.

ACKNOWLEDGMENTS

This work was supported by DFG, ME 1380/16-1.

REFERENCES

(1) Kind, H.; Yan, H. Q.; Messer, B.; Law, M.; Yang, P. D. *Adv. Mater.* **2002**, *14*, 158.
(2) Patolsky, F.; Timko, B. P.; Yu, G. H.; Fang, Y.; Greytak, A. B.; Zheng, G. F.; Lieber, C. M. *Science* **2006**, *313*, 1100.
(3) Sirbuly, D. J.; Tao, A.; Law, M.; Fan, R.; Yang, P. D. *Adv. Mater.* **2007**, *19*, 61.
(4) Wan, Q.; Li, Q. H.; Chen, Y. J.; Wang, T. H.; He, X. L.; Li, J. P.; Lin, C. L. *Appl. Phys. Lett.* **2004**, *84*, 3654.
(5) Zhang, A.; You, S. F.; Soci, C.; Liu, Y. S.; Wang, D. L.; Lo, Y. H. *Appl. Phys. Lett.* **2008**, *93*, 12110.
(6) Choi, H.; Kuno, M.; Hartland, G. V.; Kamat, P. V. *J. Mater. Chem. A* **2013**, *1*, 5487.
(7) Borgstrom, M. T.; Wallentin, J.; Heurlin, M.; Falt, S.; Wickert, P.; Leene, J.; Magnusson, M. H.; Deppert, K.; Samuelson, L. *IEEE J. Sel. Top. Quantum Electron.* **2011**, *17*, 1050.
(8) Hwang, Y. J.; Boukai, A.; Yang, P. D. *Nano Lett.* **2009**, *9*, 410.
(9) McAlpine, M. C.; Ahmad, H.; Wang, D. W.; Heath, J. R. *Nat. Mater.* **2007**, *6*, 379.
(10) Wallentin, J.; Anttu, N.; Asoli, D.; Huffman, M.; Aberg, I.; Magnusson, M. H.; Siefer, G.; Fuss-Kailuweit, P.; Dimroth, F.; Witzigmann, B.; Xu, H. Q.; Samuelson, L.; Deppert, K.; Borgstrom, M. T. *Science* **2013**, *339*, 1057.
(11) Hahm, J.; Lieber, C. M. *Nano Lett.* **2004**, *4*, 51.
(12) Zheng, G. F.; Lu, W.; Jin, S.; Lieber, C. M. *Adv. Mater.* **2004**, *16*, 1890.
(13) Zheng, G. F.; Patolsky, F.; Cui, Y.; Wang, W. U.; Lieber, C. M. *Nat. Biotechnol.* **2005**, *23*, 1294.
(14) Wagner, R. S.; Ellis, W. C. *Appl. Phys. Lett.* **1964**, *4*, 89.
(15) Wang, F. D.; Dong, A. G.; Sun, J. W.; Tang, R.; Yu, H.; Buhro, W. E. *Inorg. Chem.* **2006**, *45*, 7511.
(16) Li, Z.; Kurtulus, O.; Fu, N.; Wang, Z.; Kornowski, A.; Pietsch, U.; Mews, A. *Adv. Funct. Mater.* **2009**, *19*, 3650.
(17) Wang, F. D.; Wayman, V. L.; Loomis, R. A.; Buhro, W. E. *ACS Nano* **2011**, *5*, 5188.
(18) Ouyang, L.; Maher, K. N.; Yu, C. L.; McCarty, J.; Park, H. *J. Am. Chem. Soc.* **2007**, *129*, 133.
(19) Kwak, W. C.; Kim, T. G.; Lee, W. J.; Han, S. H.; Sung, Y. M. *J. Phys. Chem. C* **2009**, *113*, 1615.
(20) Dorn, A.; Wong, C. R.; Bawendi, M. G. *Adv. Mater.* **2009**, *21*, 3479.
(21) Sung, Y. M.; Kwak, W. C.; Kim, T. G. *CrystEngComm* **2012**, *14*, 389.
(22) Lu, X. M.; Hanrath, T.; Johnston, K. P.; Korgel, B. A. *Nano Lett.* **2003**, *3*, 93.
(23) Cui, Y.; Lauhon, L. J.; Gudiksen, M. S.; Wang, J. F.; Lieber, C. M. *Appl. Phys. Lett.* **2001**, *78*, 2214.
(24) Wang, D. W.; Dai, H. J. *Angew. Chem., Int. Ed.* **2002**, *41*, 4783.
(25) Laocharoensuk, R.; Palaniappan, K.; Smith, N. A.; Dickerson, R. M.; Werder, D. J.; Baldwin, J. K.; Hollingsworth, J. A. *Nat. Nanotechnol.* **2013**, *8*, 660.
(26) Fu, N.; Li, Z.; Myalitsin, A.; Scolari, M.; Weitz, R. T.; Burghard, M.; Mews, A. *Small* **2010**, *6*, 376.
(27) Martinez, G. T.; Zavala, G.; Videa, M. *J. Mex. Chem. Soc.* **2009**, *53*, 7.
(28) Bian, J. C.; Li, Z.; Chen, Z. D.; He, H. Y.; Zhang, X. W.; Li, X.; Han, G. R. *Appl. Surf. Sci.* **2011**, *258*, 1831.
(29) Brulle, T.; Denisenko, A.; Sternschulte, H.; Stimming, U. *Phys. Chem. Chem. Phys.* **2011**, *13*, 12883.
(30) Hezard, T.; Fajerwerg, K.; Evrard, D.; Colliere, V.; Behra, P.; Gros, P. *Electrochim. Acta* **2012**, *73*, 15.
(31) Yu, A. M.; Wang, Q. X.; Yong, J. W.; Mahon, P. J.; Malherbe, F.; Wang, F.; Zhang, H. L.; Wang, J. M. *Electrochim. Acta* **2012**, *74*, 111.
(32) Sandmann, G.; Dietz, H.; Plieth, W. *J. Electroanal. Chem.* **2000**, *491*, 78.
(33) Ueda, M.; Dietz, H.; Anders, A.; Kneppe, H.; Meixner, A.; Plieth, W. *Electrochim. Acta* **2002**, *48*, 377.
(34) Scheludko, A.; Todorova, M. *Izv. Bulg. Akad. Nauk., Otd. Fiz.-Mat. Tekh. Nauki, Ser. Fiz.* **1952**, *3*, 61.
(35) Ustarroz, J.; Ke, X. X.; Hubin, A.; Bals, S.; Terryn, H. *J. Phys. Chem. C* **2012**, *116*, 2322.
(36) Penner, R. M. *J. Phys. Chem. B* **2001**, *105*, 8672.
(37) Liu, H.; Favier, F.; Ng, K.; Zach, M. P.; Penner, R. M. *Electrochim. Acta* **2001**, *47*, 671.
(38) Riveros, G.; Vasquez, J.; Gomez, H.; Makarova, T.; Silva, D.; Marotti, R. E.; Dalchiele, E. A. *Appl. Phys. A: Mater. Sci Process.* **2008**, *90*, 423.
(39) Li, Z.; Kornowski, A.; Myalitsin, A.; Mews, A. *Small* **2008**, *4*, 1698.
(40) Li, Z.; Ma, X. D.; Sun, Q. A.; Wang, Z.; Liu, J. A.; Zhu, Z. H.; Qiao, S. Z.; Smith, S. C.; Lu, G. Q.; Mews, A. *Eur. J. Inorg. Chem.* **2010**, 4325.

(41) Wang, Z.; Li, Z.; Kornowski, A.; Ma, X. D.; Myalitsin, A.; Mews, A. *Small* **2011**, *7*, 2464.
(42) Schafer, S.; Wang, Z.; Zierold, R.; Kipp, T.; Mews, A. *Nano Lett.* **2011**, *11*, 2672.